Biaxial deformation of a polymer under shear: NMR test of the Doi-Edwards model with convected constraint release

Ryan J. Cormier,[1] Maria L. Kilfoil,[2] and Paul T. Callaghan[1]
[1]*Institute of Fundamental Sciences–Physics, Massey University, Palmerston North, New Zealand*
[2]*Department of Physics and Physical Oceanography, Memorial University of Newfoundland, St. Johns, Newfoundland, Canada A1B 3X7*

(Received 16 May 2001; revised manuscript received 14 August 2001; published 30 October 2001)

^{2}H NMR quadrupole interaction spectroscopy has been used to measure the deformation of a 670 kD poly(dimethylsiloxane) melt under shear in a Couette cell. The signals were acquired from a per deuterated benzene probe molecule which provides a motionally averaged sampling of the entire segmental ensemble. We have measured the dependence on shear rate of the S_{XX} (velocity), S_{YY} (velocity gradient), S_{ZZ} (vorticity), and S_{XY} (shear) elements of the segmental alignment tensor, as well as the angular dependence of the deuterium quadrupole splitting at fixed shear rate. We show that the data agree quite well with the Doi-Edwards theory but significantly better when convected constraint release effects are included. These fits return a value for the tube disengagement time of 100 ms.

DOI: 10.1103/PhysRevE.64.051809 PACS number(s): 36.20.−r

INTRODUCTION

The deformation of a random coil polymer under shear may be described by means of the averaged segmental alignment tensor [1,2]

$$S_{\alpha\beta}(t)=L^{-1}\int_0^L ds\langle u_\alpha(s,t)u_\beta(s,t)-\tfrac{1}{3}\delta_{\alpha\beta}\rangle, \qquad (1)$$

where the u_α are α components of tangent vectors to the segments, $\langle\cdots\rangle$ represents the ensemble average, and the integral is taken over the curvilinear path of s chain segments along the chain length L. Recently, we have shown that it is possible [3,4] to use deuterium nuclear magnetic resonance (NMR) spectroscopy to measure elements of $S_{\alpha\beta}$, in particular obtaining the diagonal elements corresponding to the velocity axis correlation S_{XX} and the velocity gradient correlation S_{YY} for a 610 kD melt of poly(dimethylsiloxane) [4]. These two terms afford some insight regarding the normal stresses. However, that earlier study was limited in three major respects. First, we obtained no measurement of the diagonal element corresponding to the vorticity axis alignment, S_{ZZ}, and so we were unable to draw conclusions regarding the biaxiality of the deformation, and, in particular, the ratio of second to first normal stress differences,

$$\frac{\Psi_2}{\Psi_1}=\left.\frac{S_{YY}-S_{ZZ}}{S_{XX}-S_{YY}}\right|_{\dot\gamma=0}. \qquad (2)$$

Second, we made no measurement of the off-diagonal element of the deformation tensor, S_{XY}, which is responsible for the shear stress. Third, we did not achieve the shear rate needed to deform the polymer sufficiently strongly (i.e., with sufficiently high Deborah number) that near-complete alignment of the polymer along the velocity axis could be induced. In the present study we extend our work to cover all these aspects, and in doing so present a comprehensive NMR study of polymer melt deformation at fixed molar mass.

The physical significance of the alignment tensor is that it is responsible for determining both optical and mechanical properties of the polymer melt. In particular, it may be directly related to elements of the stress tensor, and it determines the optical anisotropy in the material refractive index $n_{\alpha\beta}$ known as birefringence, via the stress-optical law $n_{\alpha\beta}=C\sigma_{\alpha\beta}$. C is called the stress-optical coefficient [2,5]. Birefringence measurements may be used [6] to investigate the segmental alignment tensor and so give some insight regarding the deformation depicted in Fig. 1. If incident plane polarized light has its polarization axis parallel to the extension axis, a unique refractive index is observed. In this case extinction will occur between polarizers crossed at some angle χ, generally called the extinction angle. In simple shear flow this angle defines the orientation of the principal axis of deformation of the polymer to the local velocity direction.

Our use of deuterium NMR to measure segmental alignment avoids some of the underlying assumptions inherent to the optical methods, for example, the identity of the macroscopic and microscopic polarizability tensors, and the dominance of intrinsic birefringence over form birefringence. In principle, the NMR method provides a direct measurement of $S_{\alpha\beta}$. However, as in birefringence studies, we do require a somewhat arbitrary scaling constant, similar to the stress-optical coefficient. Our approach relies on a measurement of the orientation of bond vectors through the strength of the electric quadrupole interaction experienced by deuterons present on a small probe molecule which rapidly samples the mean alignment of the host polymer. The strength of this interaction depends in a very simple manner upon the relative orientation of the electric field gradient axis (the bond axis) and the polarizing magnetic field used to produce the nuclear Zeeman effect. Because of the use of an indirect probe, the measurement of alignment is not absolute; hence the need for the scaling constant. However, the relative values of the quadrupole interaction strength precisely follow the defined tensor elements, given appropriate alignment of the magnetic field with respect to the hydrodynamic axes being investigated. Consequently, we are able to make an accurate quantitative test of microscopic models, such as the Doi-Edwards theory and its several variants.

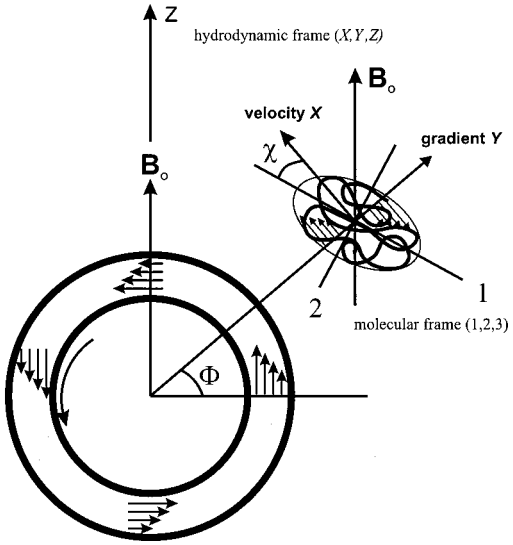

FIG. 1. Schematic diagram of a horizontal Couette cell in which the vorticity axis is aligned normal to the magnetic field. The molecular and hydrodynamic frames are shown for a region of the fluid in which the angle between the local velocity direction and the magnetic field is given by Φ. The angle between the principal axis of the molecular (1,2,3) frame and the velocity axis X is the extinction angle χ.

THEORY

Measurement of segmental alignment by NMR

The details of our NMR method have been given elsewhere [4,7]. It utilizes the electric quadrupole interaction experienced by a deuterium nucleus hosted by a hydrogen atom in an anisotropic electronic environment. In our case we use the deuteron in perdeuteriobenzene (C_6D_6). This probe molecule is introduced to the polymer melt at low concentration ($\sim$10% w/w), and, because of local steric effects, is sensitive to local polymer segment orientation [8–10]. Thus the probe inherits some of the orientation present in the polymer when the matrix material is aligned in deformational flow [8]. Because the probe molecule diffuses rapidly, it samples an ensemble-averaged order according to Eq. (1). This averaging is performed over a characteristic diffusion length determined by the benzene diffusion coefficient and the time scale associated with the quadrupole interaction strength (a few tens of hertz). This distance, at several micrometers, is much larger than the molecular scale, so that the ensemble average of segmental alignment is indeed performed over a large number of polymer molecules.

In NMR experiments the reference axis for orientation is provided by the direction of the main polarizing magnetic field. Because the nuclear magnetic dipole (Zeeman) interactions with this field are overwhelmingly dominant, they define the spin quantization axis z along which the electric quadrupole interaction is projected as a first order perturbation [11].

The effect of the electric quadrupole interaction is to split the deuterium resonance into a doublet separated in frequency by $(\frac{3}{2}eV_{zz}Q/h)P_2(\cos\theta)$, where V_{zz} is the electric field gradient strength, Q is the nuclear quadrupole moment, θ is the angle between the field gradient axis and the polarizing magnetic field, and $P_2(\cos\theta)$ is the second rank Legendre polynomial [11]. Of course, θ corresponds to the angle that the local C-D bond in the benzene subtends with the magnetic field. This rapidly fluctuates as the probe molecule tumbles and migrates in rotational and translational Brownian motion. Suppose that the tangent vector to a local polymer segment is oriented at angle α to the magnetic field. This axis effectively defines the director of a local ''nematic'' environment. The probe molecule, which has a fluctuating orientation $(\theta_\alpha,\phi_\alpha)$ with respect to this director, thus exhibits a scaled down quadrupole splitting associated with that local site via a ''pseudonematic'' interaction, exactly akin to the local anisotropic steric interactions experienced by small probe molecules placed in a nematic liquid crystal [9,10]. The average value $\overline{P_2(\cos\theta_\alpha)}$ therefore defines a local order parameter that scales the quadrupole interaction strength. Thus the quadrupole splitting may be written

$$\Delta\nu=\left(\frac{3}{2}\frac{eV_{zz}Q}{h}\right)\overline{P_2(\cos\theta_\alpha)}S_{zz}, \tag{3}$$

where $S_{zz}=L^{-1}\int_0^L ds\langle u_z(s)u_z(s)-\frac{1}{3}\rangle$, and is identically the ensemble average of $P_2(\cos\alpha)$.

When considering the deformation of a polymer under shear, the alignment tensor $S_{\alpha\beta}$ is naturally defined in a hydrodynamic reference frame whose axes are given by the velocity (X), velocity gradient (Y), and vorticity (Z) directions. However, the deformation of the polymer can also be described in a principal molecular axis frame (1,2,3) in which the alignment tensor is diagonal and given by

$$S_{\text{principal}}=\begin{pmatrix} S_{11} & 0 & 0\\ 0 & S_{22} & 0\\ 0 & 0 & S_{33}\end{pmatrix}, \tag{4}$$

where $S_{11}+S_{22}+S_{33}=0$. The 3 axis of the molecule is designated to be coincident with the vorticity axis Z. One model that is able to give a quantitative description of S is the Doi-Edwards theory [1,2]. In this theory, the deformation of the molecule is biaxial, i.e., $S_{22}\neq S_{33}$. By contrast, in the case of a uniaxial deformation, $S_{22}=S_{33}=-S_{11}/2$. The orientation of the (1,2,3) frame with respect to the hydrodynamic frame is described by a rotation about the 3 axis by the so-called ''extinction angle'' χ, as shown in Fig. 1. Thus the alignment tensor $S_{\alpha\beta}$ in the hydrodynamic frame is given by

$$\begin{aligned}\begin{pmatrix} S_{XX} & S_{XY} & 0\\ S_{XY} & S_{YY} & 0\\ 0 & 0 & S_{ZZ}\end{pmatrix}&=\begin{pmatrix} \cos\chi & -\sin\chi & 0\\ \sin\chi & \cos\chi & 0\\ 0 & 0 & 0\end{pmatrix}\\ &\times\begin{pmatrix} S_{11} & 0 & 0\\ 0 & S_{22} & 0\\ 0 & 0 & S_{33}\end{pmatrix}\\ &\times\begin{pmatrix} \cos\chi & \sin\chi & 0\\ -\sin\chi & \cos\chi & 0\\ 0 & 0 & 0\end{pmatrix}.\end{aligned} \tag{5}$$

From Eq. (5), it may be easily shown that $\chi = \frac{1}{2}\tan^{-1}[2S_{XY}/(S_{XX}-S_{YY})]$.

In order to relate elements of the hydrodynamic frame tensor $S_{\alpha\beta}$ to those measured through the NMR quadrupole interaction experiment, it is necessary to transform into the frame of the magnetic field, i.e.,

$$R(\Theta,\Phi)\begin{pmatrix} S_{XX} & S_{XY} & 0 \\ S_{XY} & S_{YY} & 0 \\ 0 & 0 & S_{ZZ} \end{pmatrix} R^{-1}(\Theta,\Phi), \tag{6}$$

where the polar angle Θ defines the direction of the vorticity axis Z relative to the magnetic field $\mathbf{B}_0$, and the angle Φ defines the orientations of X and Y in the plane normal to Z.

In the NMR experiments described here, two types of measurement are possible. In the first, we use a Couette cell with the vorticity direction oriented along $\mathbf{B}_0$, whose direction we assign the coordinate z. Thus we are able measure S_{ZZ} directly. In the second, the vorticity axis is oriented transverse to the field and we measure a projection along $\mathbf{B}_0$ in the X-Y (velocity–velocity gradient) plane. We are able to choose the orientation Φ of the velocity axis with respect to $\mathbf{B}_0$ by means of a selective excitation method in which deuteron NMR spectra are observed from a predetermined arc within the Couette cell [12]. Consequently, the z-projected alignment $S_{zz}(\Phi)$ measured in the NMR experiment is related to the hydrodynamic frame elements by

$$S_{zz}(\Phi) = S_{XX}\cos^2\Phi - 2S_{XY}\sin\Phi\cos\Phi + S_{YY}\sin^2\Phi. \tag{7}$$

Equation (7) illustrates how the elements S_{XX}, S_{YY}, and S_{XY} may each be measured, the first two by setting $\Phi = 0$ and $\pi/2$ respectively, and the last by setting $\Phi = \pi/4$ and noting

$$S_{XY} = 0.5[S_{zz}(0) + S_{zz}(\pi/2)] - S_{zz}(\pi/4). \tag{8}$$

We further note that when the deformation is uniaxial Eq. (5) may be used to show that $S_{zz}(\Phi)$ reduces to the Legendre polynomial $P_2(\cos(\Phi-\chi))$. Deviations of the angular variation from this form provide one measure of biaxiality.

The model of Doi and Edwards describes the many entanglements of a flexible polymer chain with its neighbors [1], incorporating de Gennes' idea of reptation [13]. In this model, polymer chains undergo a spectrum of relaxational translational motions largely directed along a tube defined by constraining entanglements with the neighboring chains. The dynamics can be roughly grouped as follows.

(i) Rapid motions with time constant τ_e corresponding to equilibration dynamics reflecting the crossover from a chain in free space to one that experiences the tube of constraints from neighboring chains. Dynamics faster than τ_e are short length scale, fast motions parametrized by a, an effective radius of the tube.

(ii) Intermediate motions, characterized by the Rouse time τ_R, for translational diffusion along the curvilinear tube path. Rouse mode fluctuations take place as the deformed chain retracts along the tube, restoring the tube's contour length.

(iii) Slow disengagement dynamics which determine the longest relaxation time τ_d, the time for chain reptation to define a new tube. The tube disengagement time scales approximately as the cube of the molecular weight. In general, $\tau_d \gg \tau_R$ for long polymer chains.

Under equilibrium conditions entangled polymer solutions and melts are isotropic. Under shear the polymer molecule deforms. The degree of deformation is determined by the competition that arises between the internal Brownian dynamics and the external deformation rate $\dot{\gamma}$. For $\dot{\gamma} \ll \tau_R^{-1}$ (corresponding to the experiments performed here) the relevant Brownian dynamics correspond to tube disengagement and the relevant dimensionless parameter is the Deborah number $\mathrm{De} = \dot{\gamma}\tau_d$. In this regime, while the average alignment of tube segments may change, the tube remains unstretched.

For $\mathrm{De} \ll 1$ the polymer conformation is weakly perturbed. The resulting ^{2}H NMR spectrum will contain a single isotropic line. For De on the order of or greater than unity there results an anisotropic distribution of segment orientations, manifested in the NMR spectrum as a dipolar or quadrupolar broadening of the line or a splitting into two lines. This splitting provides not only a signature of anisotropy, but also a direct measure of elements of the segmental alignment tensor.

The nonthermal reorientational motions of the chain segments driven by the applied macroscopic velocity field are accounted for in the expression for the stress tensor [2]

$$\sigma_{\alpha\beta}(t) = \frac{c}{N}\frac{3k_BTL}{Nb^2}\int_0^L ds\langle u_\alpha(s,t)u_\beta(s,t) - \tfrac{1}{3}\delta_{\alpha\beta}\rangle. \tag{9}$$

In consequence, the expression for the stress tensor is closely related to the alignment tensor. Indeed, in the Doi-Edwards formulation, $\sigma_{\alpha\beta}(t)$ is directly proportional to $S_{\alpha\beta}(s,t)$, averaged over the polymer segments [Eq. (1)]. For steady shear flow it is therefore sufficient to find an expression for the (shear-rate-dependent) segmental alignment tensor in order to evaluate the response functions such as shear stress, normal stresses, and viscosity.

The ensemble-averaged segmental alignment depends entirely on the history of the deformation and of the relaxation, obtained as an integral over past time:

$$S_{\alpha\beta}(t) = \int_{-\infty}^{t} dt' \left(\frac{\partial}{\partial t'}\psi(t-t')\right) Q_{\alpha\beta}^{(\mathrm{IA})}(\mathbf{E}(t,t')), \tag{10}$$

where $\psi(t)$ is the usual Doi-Edwards relaxation function for tube disengagement,

$$\psi(t) = \sum_{p\ \mathrm{odd}} \frac{8}{p^2\pi^2}\exp(-p^2t/\tau_d). \tag{11}$$

$Q_{\alpha\beta}$ describes the distribution of segment orientations as a function of the deformation gradient history tensor $\mathbf{E}(t,t')$, $Q_{\alpha\beta}^{(\mathrm{IA})}$ being evaluated using the independent alignment (IA) approximation for the tube orientation distribution. This approximation is employed in the model to sim-

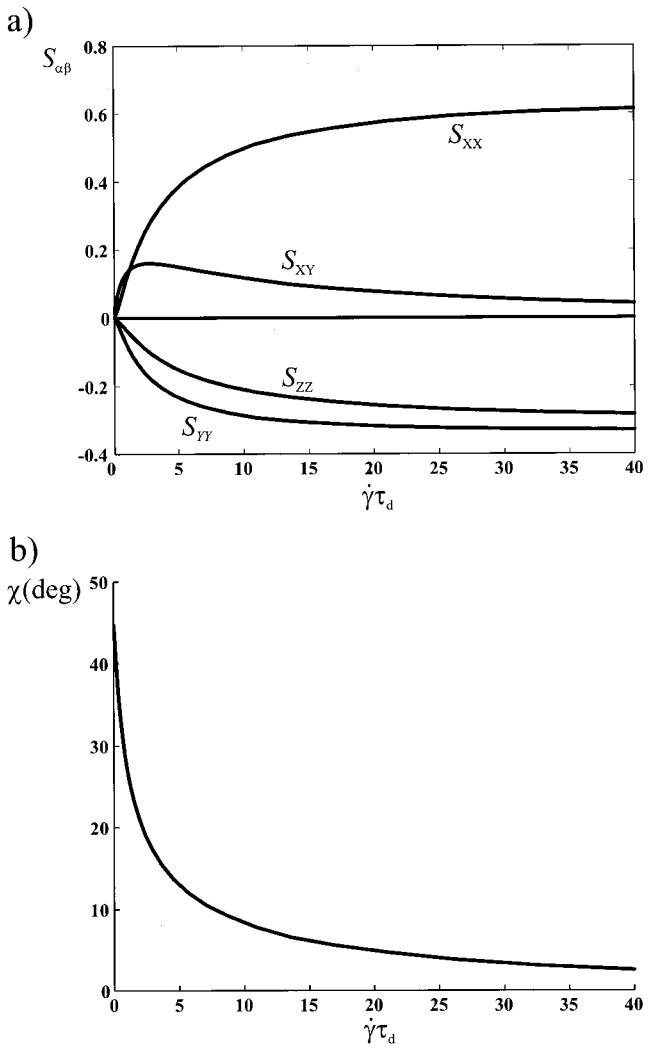

FIG. 2. (a) Elements of the alignment tensor $S_{\alpha\beta}$, in terms of the reduced shear rate $\dot{\gamma}\tau_d$, as calculated from the Doi-Edwards theory. (b) Extinction angle χ, in terms of the reduced shear rate $\dot{\gamma}\tau_d$, as calculated from the Doi-Edwards theory.

plify the way the averaging over the solid angle is carried out, and will be discussed further below.

The stress tensor is written

$$\sigma_{\alpha\beta}(t) = G_e S_{\alpha\beta}(t), \tag{12}$$

where $G_e = 3k_B T c b^2/a^2$ is the relaxation modulus, which depends on material properties, b being the statistical segment length and c the number of segments per volume. Thermodynamic dependence is explicit in G_e, and is implicit in the thermal modes of relaxation that contribute to $\psi(t)$. The above expression for $\sigma_{\alpha\beta}$ [Eq. (12)] and an appropriate probability function $\psi(t)$ together form the constitutive equation for concentrated solutions and melts.

Predictions of the Doi-Edwards model

The solution for $S_{\alpha\beta}$ in Eq. (10) has been evaluated using the standard reptation expression for $\psi(t)$ as given in Eq. (11). Figure 2(a) shows the independent alignment predictions for $S_{\alpha\beta}$ under steady shear. Note that $S_{\alpha\beta}$ is traceless so that S_{XX}, S_{YY}, and S_{ZZ} sum to zero for all values of De.

Consequences of the Doi-Edwards model are that (1) $S_{YY} \neq S_{ZZ}$, in other words $\sigma_{YY} \neq \sigma_{ZZ}$; the deformation in steady shear is biaxial; and (2) with increasing shear rate, the shear stress S_{XY} increases; beyond $\dot{\gamma}\tau_d \sim 1$, S_{XY} begins to decrease slowly toward zero. The biaxial nature of the normal stresses is well known. However, prediction 2 is not generally observed experimentally. In melts and concentrated solutions the shear stress tends to reach a plateau above De$\sim$1 and does not approach zero. Thus the bare Doi-Edwards model underpredicts the shear stress for De >1. This has a significant consequence for the extinction angle χ. Figure 2(b) shows the calculated shear rate dependence of the extinction angle χ in the Doi-Edwards model. As $\dot{\gamma}$ increases, χ decreases from its initial value of 45° to an asymptotic value near zero, indicating that the polymer is oriented along X for De$\gg$1. Note that the extinction angle, which is measured directly in birefringence studies, can also be expressed in terms of the stress via the stress-optical law as $\chi = \frac{1}{2}\tan^{-1}([2\sigma_{XY}/(\sigma_{XX} - \sigma_{YY})])$.

The independent alignment approximation

The IA approximation involves a decoupling of the average over the isotropic distribution of unit vectors **u** (the average being indicated by $\langle \cdots \rangle_0$), in the following [9]:

$$\begin{aligned} Q_{\alpha\beta}(\mathbf{E}) &= \left\langle \frac{(\mathbf{E}\cdot\mathbf{u})_\alpha (\mathbf{E}\cdot\mathbf{u})_\beta}{|\mathbf{E}\cdot\mathbf{u}|} \right\rangle_0 \frac{1}{\langle |\mathbf{E}\cdot\mathbf{u}| \rangle_0} - \frac{1}{3}\delta_{\alpha\beta} \\ &\cong \left\langle \frac{(\mathbf{E}\cdot\mathbf{u})_\alpha (\mathbf{E}\cdot\mathbf{u})_\beta}{|\mathbf{E}\cdot\mathbf{u}|^2} - \frac{1}{3}\delta_{\alpha\beta} \right\rangle_0 \\ &\equiv Q^{(\mathrm{IA})}_{\alpha\beta}(\mathbf{E}). \end{aligned} \tag{13}$$

Although the error introduced in the IA approximation is small [2], some improvement in the model is made by avoiding this step [15,16]. We have recalculated the Doi-Edwards predictions without using IA, that is, by using the left hand side in Eq. (13). The independent alignment approximation is removed by performing the sum over the solid angle separately for $(\mathbf{E}\cdot\mathbf{u})_\alpha (\mathbf{E}\cdot\mathbf{u})_\beta/|\mathbf{E}\cdot\mathbf{u}|$ and $1/|\mathbf{E}\cdot\mathbf{u}|$, to arrive at $Q_{\alpha\beta}(\mathbf{E})$. Figures 3(a) and 3(b) show these latter calculations as solid curves. The difference without IA is mainly in the enhancement of S_{XX} and S_{ZZ}, and a more pronounced maximum in the shear stress around De$\sim$1. Because the magnitudes of the normal stresses are changed with IA removed, the limiting behavior of the ratio of second to first normal stress difference as the strain goes to zero [Eq. (2)] becomes $-\frac{1}{7}$, versus $-\frac{2}{7}$ for the Doi-Edwards model with the independent alignment approximation [2]. In what follows we shall refer to the model with the IA approximation as the bare Doi-Edwards model and that without the IA approximation as Doi-Edwards ($-$IA).

Modified De: Convected constraint release

While the Doi-Edwards theory works well in a number of respects, there remain some problems. These include the un-

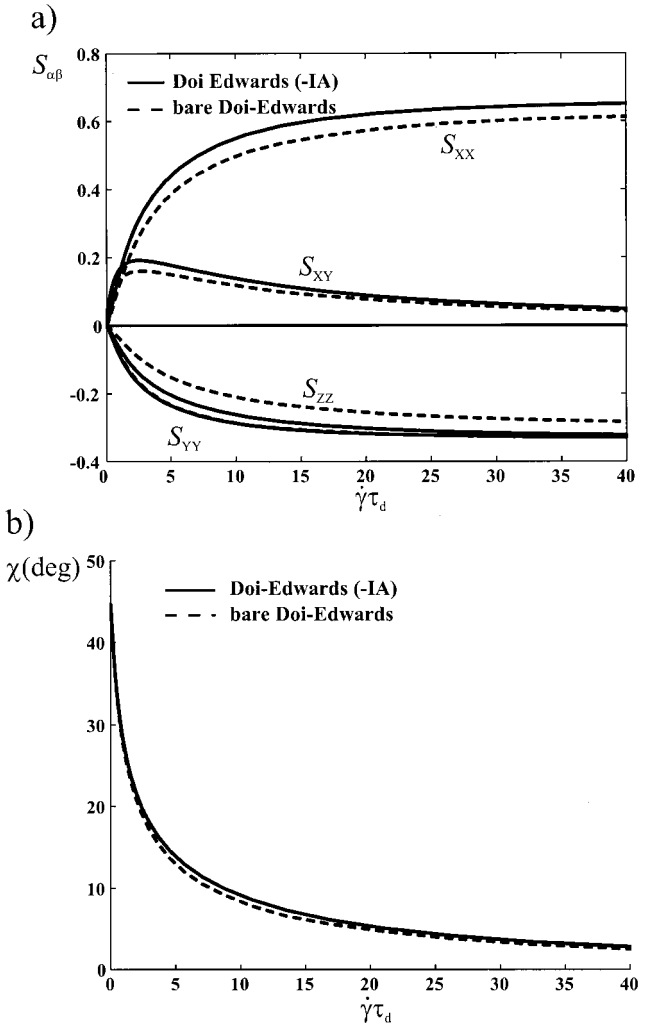

FIG. 3. (a) Elements of the alignment tensor $S_{\alpha\beta}, \sigma_{\alpha\beta}$, in terms of the reduced shear rate $\dot{\gamma}\tau_d$, calculated from the Doi-Edwards theory without the independent alignment approximation (——). As a comparison the bare the Doi-Edwards theory (----) is shown as well. (b) Extinction angle χ, in terms of the reduced shear rate $\dot{\gamma}\tau_d$, as calculated from the Doi-Edwards theory without the independent alignment approximation (——).

derestimation of the shear stress and the orientation angle χ in the nonlinear regime ($\mathrm{De} \gg 1$), and the failure to correctly predict the ratio of second to first normal stress difference in shear [14–18]. Several sophisticated modifications to the model have been suggested so as to achieve a more complete theory. These include allowance for contour length fluctuations [19,20], convected constraint release [21,22], and nonaffine tube deformation [18]. We choose to incorporate the convected constraint release modification first suggested by Marrucci [21], because the effects it accounts for are important in the range $1/\tau_d < \dot{\gamma} < 1/\tau_R$ covered by our melt experiments.

The basic idea underlying convected constraint release (CCR) is that constraints to thermal motion, which arise from topological interactions with similar chains, are removed through nonthermal relative motion of the chains. The entanglements are themselves being convected away on the time scale of the flow. The constraints thus become released, providing an additional relaxation mechanism available to the chain.

CCR is incorporated into the Doi-Edwards model by assuming that the thermal and convective relaxation processes act in parallel, following Ref. [22], Eq. (12). In Eqs. (10) and (3) above and for shear rate $\dot{\gamma}$ in the plane (X, Y), the relaxation times τ are replaced with τ_{CCR} where [22]

$$\frac{1}{\tau_{\mathrm{CCR}}} = \frac{1}{\tau} + \dot{\gamma}\langle u_X u_Y \rangle. \tag{14}$$

$\dot{\gamma}\langle u_X u_Y \rangle$ is the rate of relative, convected motion of neighboring chains. $\langle u_X u_Y \rangle$ is simply S_{XY}, which we already calculate in the Doi-Edwards model. In slow flows where $\dot{\gamma} < 1/\tau_d$ the convective term can be neglected and $\tau_{\mathrm{CCR}} = \tau$. The stress tensor is then the same as that obtained using the unmodified Doi-Edwards theory. Where $\dot{\gamma}$ is comparable to $1/\tau_d$ the convective term is significant and the Doi-Edwards curves are modified. At high shear rates $\dot{\gamma}$ dominates, i.e., $\tau_{\mathrm{CCR}} \sim 1/\dot{\gamma} S_{XY}$, and the relaxation rate becomes independent of even the longest relaxation time τ_d. In what follows we shall refer to the model with CCR modification as Doi-Edwards (+CCR).

The incorporation of CCR is subtle, and we here elaborate on its implementation. In our numerical evaluation, the reduced shear rate $\dot{\gamma}\tau_d$ is stepped through a series of values and the elements of $S_{\alpha\beta}$ are calculated for each value. Time dependence appears in both $\psi(t-t')$ and $Q_{\alpha\beta}\mathbf{E}$, in the integral Eq. (10). $\partial\psi(t-t')/\partial t'$ is calculated using the first five terms in the expansion, with the first term (corresponding to slowest dynamics) dominant; and the integral is performed over a range $\tau = (t-t')$ from $\tau_d/5$ to $10\tau_d$. The alignment tensor $Q_{\alpha\beta}$ also depends on history, through $\mathbf{E}$, and for each value of $\dot{\gamma}\tau_d$ the strain history is evaluated over these same times, with the velocity gradient $\dot{\gamma}$ constant for each step. In CCR the relaxation times are shortened depending on $\dot{\gamma}$ and on the current S_{XY} orientation state, according to Eq. (14). τ is changed to τ_{CCR} in both ψ and $Q_{\alpha\beta}$, and for each value of $\dot{\gamma}\tau_d$ a new spectrum of relaxation times τ_{CCR} is calculated using S_{XY} from the previous step, with $S_{XY} = 0$ chosen for the first step. The multiexponential function $\psi(t-t')$ thus describes both thermal and convective relaxation. We note that τ_d remains implicit in the model and may be estimated from fitting the alignment tensor data.

The alignment tensor elements calculated using the CCR modification are plotted in Fig. 4(a) as solid lines. Again, the bare Doi-Edwards curves are shown as dashed lines for comparison. The most striking consequence of the Doi-Edwards (+CCR) model is that above $\dot{\gamma} \sim 1/\tau_d$ the shear stress does not go to zero and instead heads toward a nonzero plateau. The calculated extinction angle χ is plotted in Fig. 4(b). In the CCR extension to the model the deformed polymer approaches an alignment of $\sim 10°$ to the velocity direction at high shear. This is dramatically different from the asymptotic zero-degree alignment for the bare Doi-Edwards model, and is much more in agreement with χ observed in birefringence [15] and in the NMR experiments reported here.

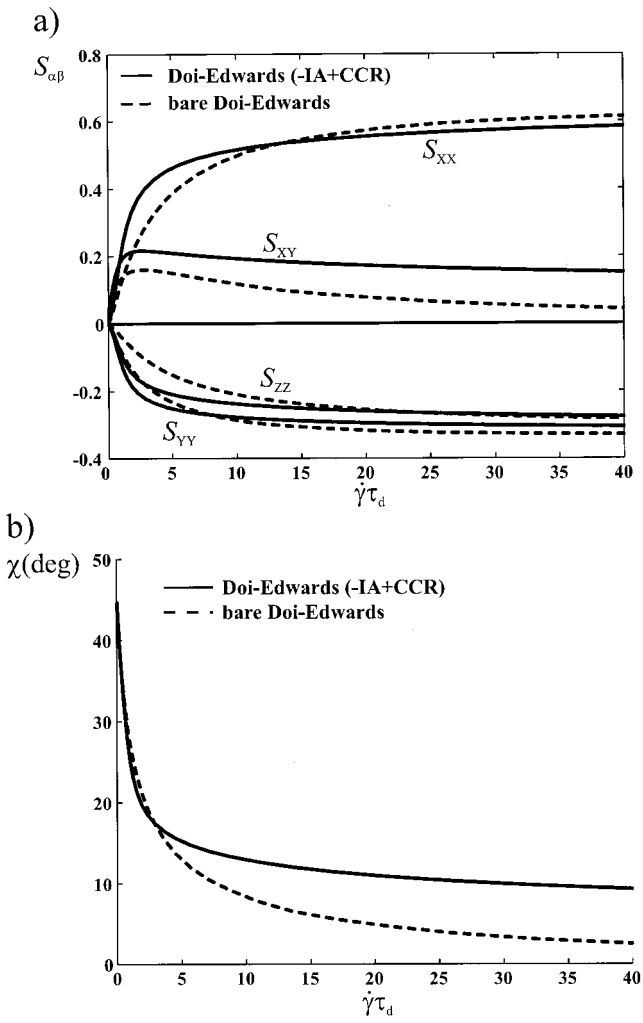

FIG. 4. (a) Elements of the alignment tensor $S_{\alpha\beta}, \sigma_{\alpha\beta}$, in terms of the reduced shear rate $\dot{\gamma}\tau_d$, calculated from the Doi-Edwards theory without the independent alignment approximation but incorporating convected constraint release (——). As a comparison the bare Doi-Edwards theory (----) is shown as well. (b) Extinction angle χ, in terms of the reduced shear rate $\dot{\gamma}\tau_d$, as calculated from the Doi-Edwards theory without the independent alignment approximation but incorporating convected constraint release (——).

The physical explanation for shear stress recovery under CCR beyond De$\sim$1 has been pointed out by Marrucci and Ianniruberto [17]. Without CCR, for De$\sim$1 the tubes become aligned along the shear direction faster than they can reform, an individual chain feels less traction from neighboring chains, and the shear stress decreases toward zero. The reptation relaxation mechanism is ''frozen out'' at high shear rates, while the convective relaxation, being proportional to $\dot{\gamma}$, does not saturate. Tubes are convected away, full alignment is suppressed, and the shear stress remains high.

EXPERIMENT

The polymer sample studied in this work is high molecular weight ($M_w = 670$ kD) poly(dimethylsiloxane) (PDMS), $M_w/M_n = 1.84$, obtained from American Polymer Standards Corporation (Cincinnati, Ohio). Approximately 10% w/w deuterated benzene (Apollo Scientific Limited, Derbyshire, U.K.) was dissolved in the sample. In order to test that the rheological properties were not significantly modified by this procedure, we made measurements of flow curves before and after addition of the deuterated benzene. The curves were obtained using a Rheometrics RS500 cone and plate cell and operating under controlled stress conditions at relatively low Deborah number in order to avoid loss of sample due to normal stress effects. The data, shown in Fig. 5, suggest that the rheological properties of the pure melt and the melt with 10% benzene are practically indistinguishable.

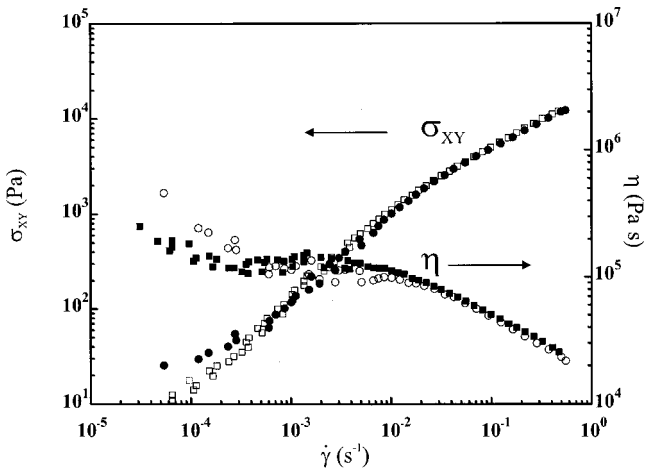

FIG. 5. Comparative flow curves for 670 kD PDMS melt at 21 °C, with (open and closed squares) and without (open and closed circles) 10% perdeuteriobenzene added.

The rheo-NMR measurements were carried out on a Bruker AMX300 spectrometer at a deuteron frequency of 46.072 MHz, using specially constructed shear cells. Figures 6(a) and 6(b) show the rheo-NMR devices used in the experiment. Figure 6(a) comprises a horizontal Couette cell

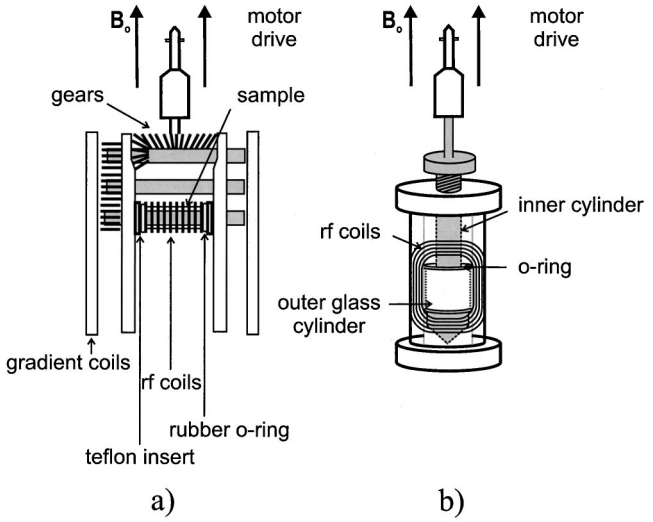

FIG. 6. Schematic diagram of (a) the horizontal Couette cell, and (b) the vertical Couette cell used in this work. A vertical shaft running down the bore of the magnet connects to the gear mechanism in the cell which is driven by a motor drive above.

made of a machinable glass (Macor) with an inner cylinder of outer diameter 5 mm and a glass outer cylinder of inner diameter 6 mm. The poly(dimethylsiloxane) is enclosed in the 0.5 mm gap between these cylinders. Figure 6(b) comprises a vertical Couette cell made entirely of PEEK (polyether ether ketone) with similar dimensions to the horizontal cell mentioned above. Surrounding the horizontal cell is a rf solenoid coil and surrounding the vertical cell is a rf saddle coil, both tuned for deuterium (^{2}H). The rheo-NMR apparatus is secured to a probe and a set of gradient coils is enclosed around the cell itself, which is then inserted into a 7.05 T superconducting magnet such that the vorticity axis is transverse to the polarizing field in the horizontal cell and oriented along $\mathbf{B}_0$ in the vertical cell. The inner cylinder of each cell is rotated by a drive shaft running down the bore of the magnet with a stepper motor mounted above. The drive shaft is in turn connected to a gear mechanism above the cell, which rotates the inner cylinder at a specified frequency.

NMR microimaging methods were used both to view the velocity distribution across the gap and to selectively excite specific regions of the sample space for spectroscopic analysis. In particular, this selection allows us to choose a region of sample in the horizontal Couette cell that corresponds to a specific alignment of the local velocity (X) axis with respect to the magnetic field, as shown in Fig. 1. The selective excitation pulse sequence has been specially devised in order to minimize exposure of selected nuclear spins to relaxation. The technique employs a selective precursor pulse sandwich that destroys magnetization outside the desired region, but stores the wanted magnetization along the z axis for later recall. Details of both the velocimetry and selective excitation methods can be found elsewhere [3,4,7]. In order to confirm that the correct region of sample is chosen, an imaging pulse module can be applied following spatial selection. Figure 7 shows three examples in which the selected region has the velocity axis coincident with, at 45° to, and normal to the polarizing $\mathbf{B}_0$ field, corresponding to angles $\Phi=0°$, 45°, and 90° in Eq. (7). Following confirmation via such images, NMR spectroscopy was performed using the identical selection precursor. The shear rates were determined from the known rotation speed of the inner cylinder and validated by velocity microimaging as shown in Fig. 8.

The spectroscopic sequence consists of a Hahn (90°_x-t_1/2-180°_y-t_1/2-acquire) echo and is used in our spectroscopy measurements in order to ensure that all unwanted Zeeman interactions arising from susceptibility inhomogeneity are refocused and the undisturbed weak quadrupolar precession is not. Thus any change in the spectrum is due entirely to quadrupolar interaction, allowing us to resolve and measure quadrupole splittings of a few hertz. The quadrupole spectrum is obtained by Fourier transformation of the echo amplitude with respect to the evolution dimension t_1.

RESULTS AND DISCUSSION

Figure 9 shows a series of ^{2}H spectra acquired for a range of shear rates in the region of the Couette cell in which the velocity axis X is aligned with the magnetic field $\mathbf{B}_0$. The spectra were obtained using the two-dimensional spectroscopy sequence given in Refs. [4], [12] and yield direct, scaled measurement of the segmental alignment tensor element S_{XX}. In addition, data were obtained for the region of the Couette cell in which the velocity gradient direction Y was parallel to the magnetic field, giving S_{YY} and, at a selective 45° angle, giving S_{XY}. Similar measurements were done for the vorticity direction Z, in which the cell is realigned with the vorticity axis coincident with the $\mathbf{B}_0$ field, giving S_{ZZ}.

Figure 10(a) shows the dependence of these splittings as a function of shear rate along with the corresponding bare Doi-Edwards alignment tensor curves plotted on the same graph. The effective quadrupole interaction strength is scaled to match the absolute alignment and the tube disengagement time is adjusted to match the reduced shear rate, $\mathrm{De}=\dot{\gamma}\tau_d$. The fit to the curves is quite good for S_{XX}, S_{YY}, and S_{ZZ} and yields a value of 210 ms for τ_d. However, a discrepancy in the fit is seen for the S_{XY} data, which reach a plateau and do not go to zero. The observed plateau behavior is in accordance with the many observations of shear stress σ_{XY} versus shear rate [23–26]. Figure 10(b) shows the same experimental set of splittings $\Delta\nu$ as a function of shear rate, but now with convected constraint release incorporated and the independent alignment approximation removed from the model. With this Doi-Edwards ($-$IA+CCR) theory, the fit to S_{XY} is much improved; instead of passing through a maximum and then decreasing rapidly toward zero, one now finds a much slower decrease with increasing shear rate. The fit to the curve is quite good for S_{XX}, S_{YY}, and S_{ZZ}, except for the initial part of S_{XX}. A consistent plateau region is not seen for the S_{XY} fit, but rather a gradual decrease in the curve at higher shear rates. CCR offers a significant improvement over the bare Doi-Edwards (DE) model. Note that the fitted value for τ_d is now different from that given by the bare DE model, and is equal to 100 ms.

The relationship expressed in Eq. (7) can be directly tested by measuring the projected tensor element $S_{zz}(\Phi)$ for different angles of selective excitation in the XY plane. Such angular dependence experiments have been carried out at two fixed shear rates: at $\mathrm{De}=1$ where nonlinear viscoelastic behavior is first expected to become important, and at $\mathrm{De}=15$, well into the plateau region of fully nonlinear viscoelastic behavior. Figure 11(a) shows the angular dependence of the splitting at $\mathrm{De}=1$ along with the corresponding Doi-Edwards curve calculated using Eq. (7). The agreement is quite good. From the results in Fig. 2(b), the extinction angle χ is predicted to be 27° at this particular Deborah number. Also plotted in Fig. 11(a) is the theoretical curve $P_2\cos(\Phi\text{-}\chi)$ that might be expected if the polymer deformation were axially symmetric. While the angle χ can be freely adjusted in this fit to give a reasonable representation of the positions of maxima and minima, the value of the splitting at the minimum is substantially underestimated. In this respect the biaxial character of the deformation as predicted by the DE model gives a far better representation. Thus, the angular dependence data of Fig. 11(a) provide independent conformation of the biaxial nature of the deformation, and clear support for the Doi-Edwards model.

Figure 11(b) shows the angular dependence data at a

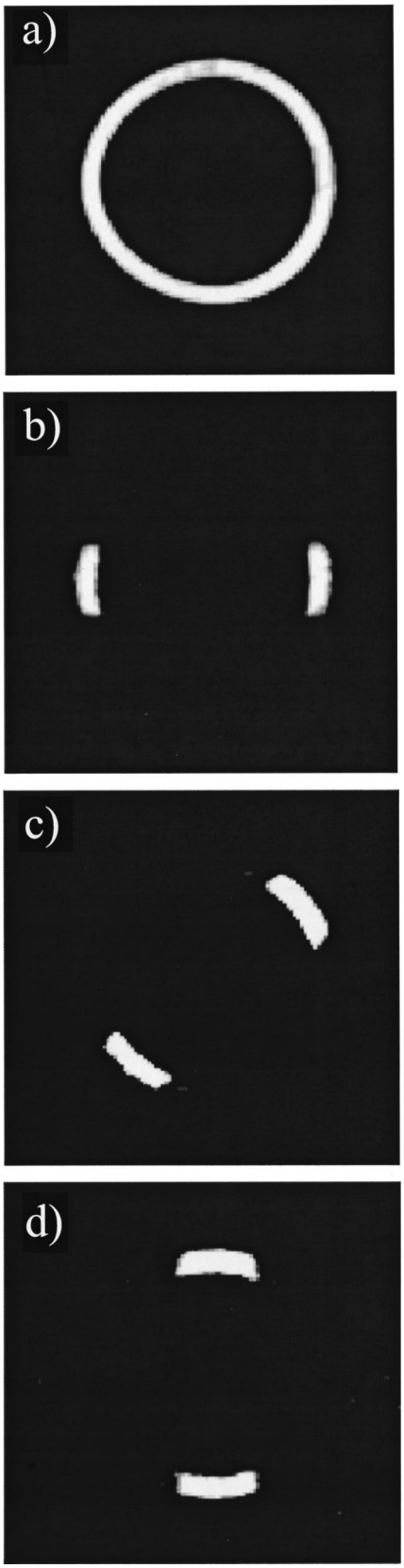

FIG. 7. NMR images obtained following the selective storage pulse sequence used to localize a part of the fluid in the horizontal Couette cell. This same sequence is used for localized NMR spectroscopy. Examples shown are for regions corresponding to angle $\Phi = 0$, 45°, and 90°.

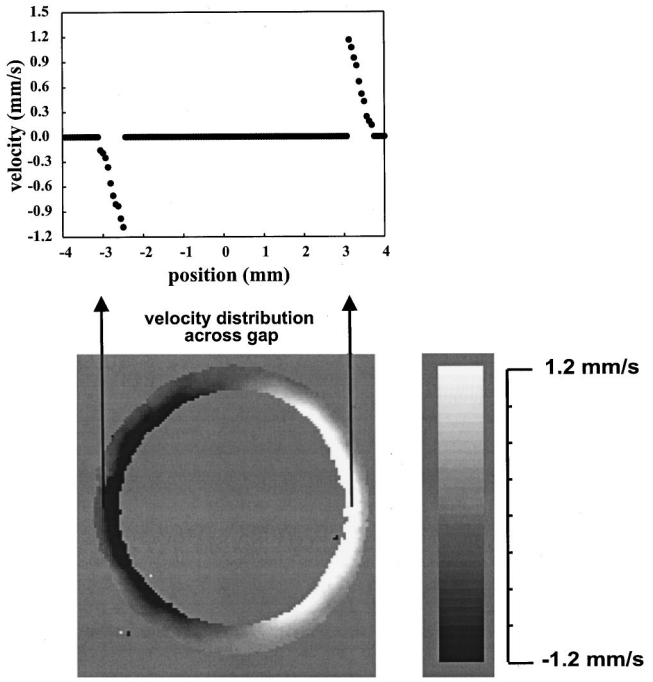

FIG. 8. NMR velocity image obtained in the horizontal Couette cell along with a profile taken across the gap. The wall velocity in this example is calculated to be around 1.2 mm/s, so that no slip is apparent in this measurement.

higher shear rate $\dot{\gamma}\tau_d = 15$, with the corresponding (unmodified) DE curve, and the CCR-modified DE curve plotted on the same graph. At these much higher Deborah numbers, the measurements of $S_{zz}(\Phi)$ reveal more subtle discrepancies in the models. For example, the data do not agree very well with the bare Doi-Edwards model for this high shear rate. This is hardly surprising, given that the discrepancy between the observed shear stress and that predicted by the unmodified Doi-Edwards model is much larger in the plateau region $\mathrm{De} \gg 1$. Because of the sensitivity of χ to S_{XY} it is inevitable that the value of χ predicted by the Doi-Edwards model will be in poor agreement with the apparent extinction angle found in the angular dependence study. Indeed, χ in the unmodified DE model is predicted to be around 6° whereas the maximum in Fig. 11(b) indicates $\chi \sim 20°$. This is much closer to the alignment angle of 14° predicted by the CCR-modified model, and the curve based on this latter model certainly gives a better depiction of the data.

Also shown in Fig. 11(b) is a fit to the data by $P_2 \cos(\Phi\text{-}\chi)$. While the value of χ can be adjusted to provide a reasonable fit, the discrepancy that remains in the value of the splitting at the minimum provides further confirmation of the biaxial character of the deformation.

Finally, in Fig. 12, we show the measured ratio of the second to the first normal stress difference, as given in Eq. (2). In most direct measurements of the normal stresses in steady shear flows of entangled polymers, the ratio of ψ_2/ψ_1 is found to lie between -0.1 and -0.3, this ratio being relatively independent of shear rate. Our results suggest a ratio of around -0.14 which is constant at low Deborah numbers, but is substantially reduced above $\mathrm{De} = 3$. We note that some

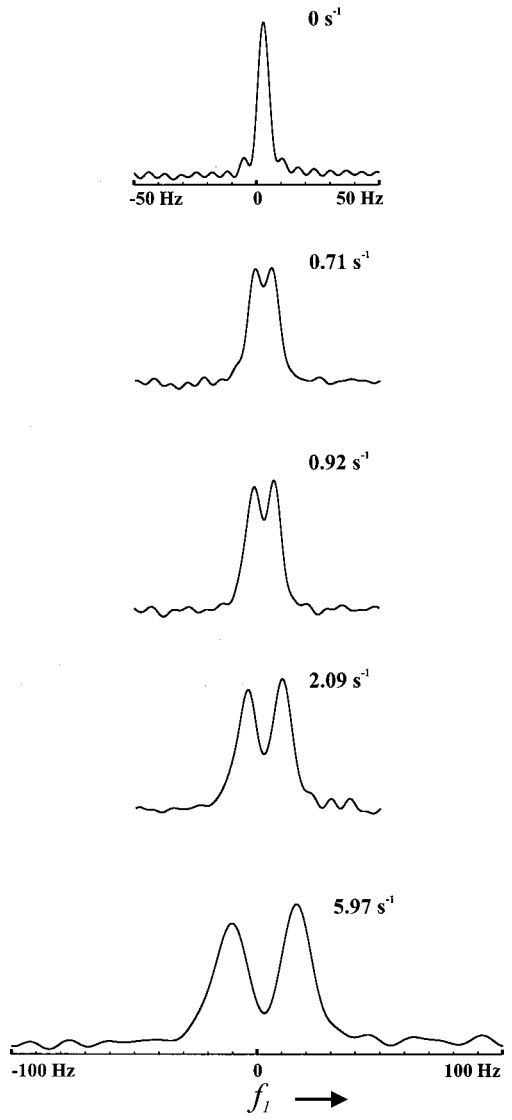

FIG. 9. ^{2}H spectra obtained for a series of shear rates by Fourier transforming the signal evolution in the t_1 domain. The spectra are plotted as signal amplitude versus frequency in hertz. The splitting arises from the electric quadrupole interaction with the $\mathbf{B}_0$ field and is a measure of orientation in the polymer under deformation.

other authors have also reported this shear thinning phenomenon in both mechanical and birefringence measurements [27–30]. The reasons for the discrepancies between the various measurements are unclear, and may be due to the differing roles of polydispersity or elastic instabilities under steady flow. However, we do attach some weight to the value of the ratio ψ_2/ψ_1 in the low Deborah number plateau. Our observation of $\psi_2/\psi_1 \approx -1/7$ is in excellent agreement with the predictions of the Doi-Edwards model without IA, with or without convected constraint release.

CONCLUSION

The Doi-Edwards model, modified to incorporate the convected constraint release mechanism and with the independent alignment approximation removed, is remarkably successful at capturing the behavior of the diagonal elements of the alignment tensor obtained by our NMR method, over the entire nonlinear range in this melt. At De<1 ($\dot{\gamma}<10$) the predictions of the CCR-modified model fall slightly below the data for all three of S_{XX}, S_{YY}, and S_{ZZ}. It is important to note that CCR modification also greatly improves the agreement of the model with the shear stress data, whereas the bare DE model fails to correctly predict the shear stress plateau. The key feature in these experiments is the determination of the complete segmental alignment tensor for this melt, over a wide shear range extending to De$\sim$10. This

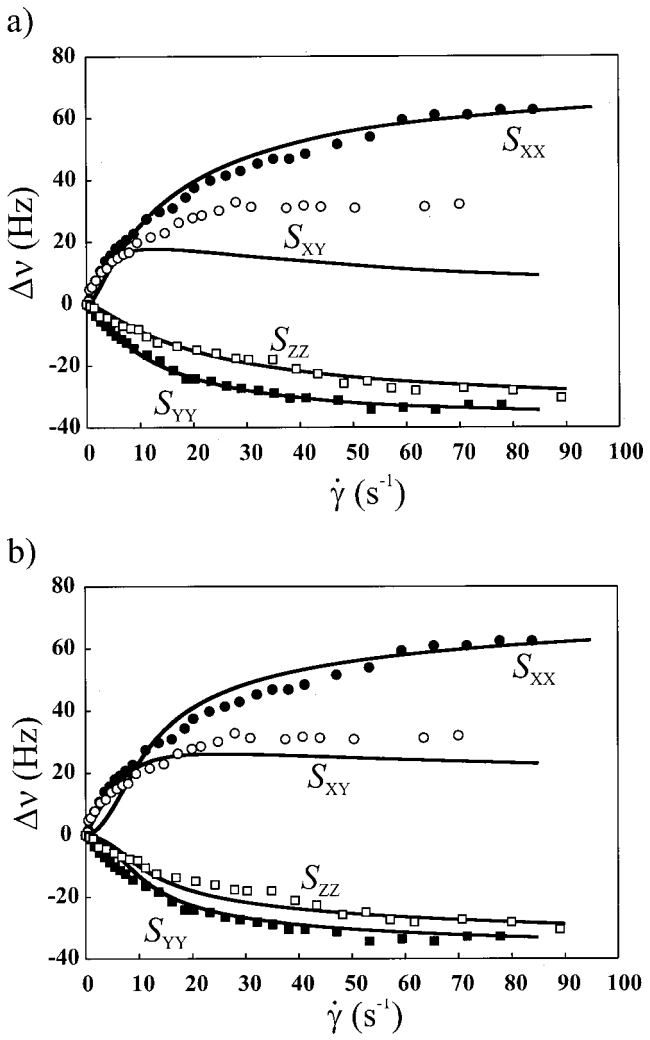

FIG. 10. (a) Deuterium quadrupole splitting $\Delta\nu$ as a function of shear rate obtained from the spectra shown in Fig. 9. Localized spectroscopy experiments were done in selected regions of the horizontal Couette cell in which the velocity direction (solid circles) and gradient direction (solid squares) are parallel to the magnetic field and at a 45° angle, giving S_{XX}, S_{YY}, and S_{XY} (open circles), respectively. Similar measurements were done in the vertical Couette cell in which the vorticity axis is parallel to the $\mathbf{B}_0$ field (open squares) giving S_{ZZ}. The best compromise Doi-Edwards fit corresponds to a τ_d of 210 ms. (b) The same segmental alignment tensor data as shown in (a), but with the best fit for the Doi-Edwards fit with CCR incorporated and IA removed. This improved fit gives $\tau_d = 100$ ms.

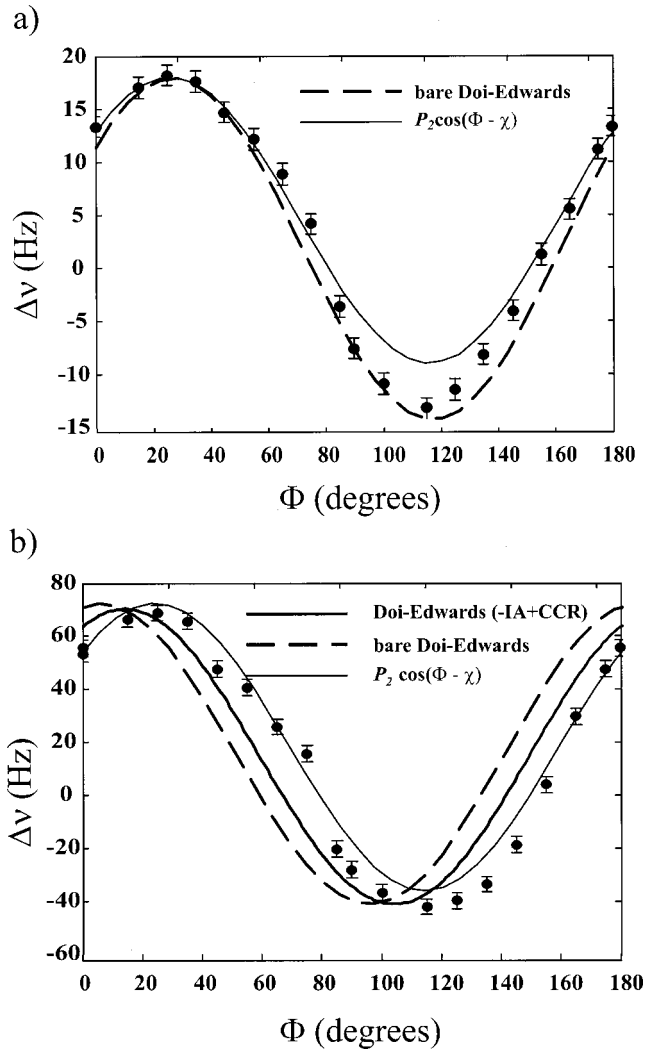

FIG. 11. (a) Quadrupole splittings $\Delta\nu$ obtained from localized spectroscopy experiments using selected regions of the horizontal Couette cell, versus orientation angle Φ and at a fixed Deborah number of $\dot{\gamma}\tau_d = 1$. The velocity axis is aligned with $\mathbf{B}_0$ at 0° and the gradient axis is aligned with $\mathbf{B}_0$ at 90°. The dashed line corresponds to the predictions of the Doi-Edwards model with the angular dependence as given by Eq. (5). The solid line shows the $P_2\cos(\Phi-\chi)$ angular dependence with χ adjusted to 27°. Note that this latter angular dependence fails to represent the biaxial nature of the deformation. (b) As for (a) but with angular dependence measurement at a fixed Deborah number of $\dot{\gamma}\tau_d = 15$. At this high shear rate, the Doi-Edwards model prediction (— — —) does not match the data well, and does not predict the correct extinction angle χ. The Doi-Edwards model with CCR incorporated and IA removed gives an improved but imperfect representation. The solid line shows the $P_2\cos(\Phi-\chi)$ angular dependence with χ adjusted to 20°.

allows for a robust test of the DE theory. In particular, we test the predicted biaxial nature of the deformation and validate the incorporation of CCR into the model. We note that for the shear rates accessed here the assumption $\dot{\gamma} \ll \tau_R^{-1}$ probably still holds, and the success of the CCR extension to the DE model in modeling the NMR data is most likely because the effects of chain stretching are not apparent here. Contour length fluctuations would become important under yet faster flows, or in melts of higher molar mass at these values of $\dot{\gamma}$, and in this case the model would require further modification to account for these effects.

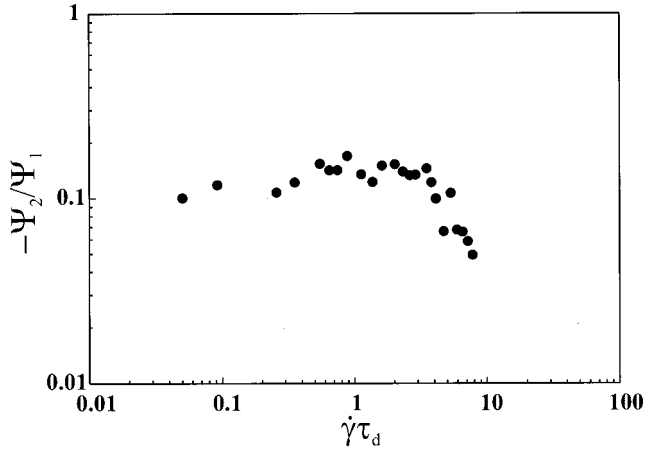

FIG. 12. Ratio of the second to the first normal stress difference, as given in Eq. (2) but calculated from the alignment tensor elements S_{XX}, S_{YY}, and S_{ZZ}. Note the reduction about De≈3.

Access to the complete alignment tensor has also provided a measure of the normal stress differences, and the results presented here display a limiting zero-shear value of -0.14 for the ratio of second to first normal stress difference. This is in excellent agreement with the exact result for the DE model with IA removed [2].

We have shown here that nuclear magnetic resonance methods based on a combination of deuteron quadrupole interaction spectroscopy and selective excitation and microimaging using specially tailored magnetic field gradient pulses have the potential to significantly enhance experimental insight regarding molecular deformation under inhomogeneous flow. The present application concerning molecular deformation in entangled polymer melts will be extended to encompass molar mass effects. However, the method is not confined to polymer melts, nor to the study of deformation in Couette flow. The NMR technique may be applied to various deformational flow geometries, while the use of an indirect probe molecule makes it possible to study alignment effects in a wide range of complex fluids.

ACKNOWLEDGMENTS

The authors are grateful to the Royal Society of New Zealand and the New Zealand Foundation for Research, Science and Technology, respectively, for funding support under the Marsden Fund and the Public Good Science Fund. M.L.K. also acknowledges financial support from the Natural Sciences and Engineering Research Council of Canada.

[1] M. Doi and S. F. Edwards, J. Chem. Soc., Faraday Trans. 2 **74**, 1802 (1978); **74**, 1818 (1978).
[2] M. Doi and S. F. Edwards, *The Theory of Polymer Dynamics* (Oxford University Press, Oxford, 1986).
[3] P. T. Callaghan, M. L. Kilfoil, and E. T. Samulski, Phys. Rev. Lett. **81**, 4524 (1998).
[4] M. L. Kilfoil and P. T. Callaghan, Macromolecules **33**, 6828 (2000).
[5] H. Janeschitz-Kriegl, *Polymer Melt Rheology and Flow Birefringence* (Springer-Verlag, New York, 1983).
[6] G. G. Fuller, *Optical Rheometry of Complex Fluids* (Oxford University Press, New York, 1995).
[7] P. T. Callaghan, *Principles of Nuclear Magnetic Resonance Microscopy* (Oxford University Press, Oxford, 1991).
[8] B. Deloche and E. T. Samulski, Macromolecules **14**, 575 (1981).
[9] E. E. Burnell and C. A. de Lange, Chem. Rev. **98**, 2359 (1998).
[10] Z. Luz, R. Poupko, and E. T. Samulski, J. Chem. Phys. **74**, 5825 (1981).
[11] A. Abragam, *The Principles of Nuclear Magnetism* (Oxford University Press, Oxford, 1961).
[12] M. L. Kilfoil and P. T. Callaghan, J. Magn. Reson. **150**, 110 (2001).
[13] P. G. de Gennes, J. Chem. Phys. **55**, 572 (1971).
[14] J. L. S. Wales, *The Application of Flow Birefringence to Rheological Studies of Polymer Melts* (Delft University Press, Rotterdam, 1976).
[15] D. W. Mead, R. G. Larson, and M. Doi, Macromolecules **31**, 7895 (1998).
[16] G. Iannirubertо and G. Marrucci, J. Non-Newtonian Fluid Mech. **79**, 225 (1998).
[17] G. Marrucci and G. Iannirubertо, J. Non-Newtonian Fluid Mech. **82**, 275 (1999).
[18] G. Marrucci, F. Greco, and G. Iannirubertо, Curr. Opin. Colloid Interface Sci. **4**, 283 (1999).
[19] M. Doi, J. Polym. Sci., Polym. Lett. Ed. **19**, 265 (1981).
[20] M. Rubinstein and S. Panyukov, Macromolecules **30**, 8036 (1997).
[21] G. Marrucci, J. Non-Newtonian Fluid Mech. **62**, 279 (1996).
[22] G. Iannirubertо and G. Marrucci, J. Non-Newtonian Fluid Mech. **65**, 241 (1996).
[23] F. J. Lim and W. R. Schowalter, J. Rheol. **33**, 1359 (1989).
[24] J. P. Gonzalez, L. P. Trejo, L. D. Vargas, and O. Manero, Rheol. Acta **36**, 677 (1997).
[25] J. P. Gonzalez and L. D. Vargas, J. Rheol. **44**, 441 (2000).
[26] H. H. Saab and R. B. Bird, J. Chem. Phys. **77**, 4758 (1982).
[27] P. Moldenaers, H. Yanase, J. Mewis, G. G. Fuller, C. S. Lee, and J. J. Magda, Rheol. Acta **32**, 1 (1993).
[28] E. F. Brown, W. R. Burghardt, H. Kahvand, and D. C. Venerus, Rheol. Acta **34**, 221 (1995).
[29] J. J. Magda, C. S. Lee, S. J. Muller, and R. G. Larson, Macromolecules **26**, 1696 (1993).
[30] J. J. Magda and S. G. Baek, Polymer **35**, 1187 (1994).